Ab initio study of the diffusion and decomposition pathways of SiH_x species on Si(100)

Michele Ceriotti,* Silvia Cereda, Francesco Montalenti, Leo Miglio, and Marco Bernasconi
Dipartimento di Scienza dei Materiali, Università di Milano-Bicocca, Via R. Cozzi 53, I-20125, Milano, Italy
(Received 5 November 2008; revised manuscript received 24 February 2009; published 28 April 2009)

Diffusion and decomposition of SiH_x species adsorbed on the clean Si(100) surface are processes of relevance for the growth of crystalline silicon by plasma-enhanced chemical vapor deposition. In this work, we report an extensive search of diffusion and decomposition pathways for SiH_3, SiH_2, and SiH by means of combined *ab initio* metadynamics simulations and optimization of minimum-energy reactions paths. We find that on the clean surface SiH_3 undergoes stepwise decompositions into Si and H adatoms according to $SiH_3 \rightarrow SiH_2 + H \rightarrow SiH + 2H \rightarrow Si + 3H$ with an overall reaction barrier of the order of 0.8 eV, consistent with the scenario inferred from secondary ion mass spectroscopy data. The lifetime of SiH_3 at room temperature calculated within transition state theory in the harmonic approximation is in agreement with experiments. The lifetime of SiH_2 turns out to be similar to that of SiH_3. Possible trap states for SiH_2 are proposed, based on energetics and by comparing calculated scanning tunneling microscope images with experimental data.

DOI: 10.1103/PhysRevB.79.165437 PACS number(s): 81.15.Gh, 68.47.Fg, 68.43.Bc

I. INTRODUCTION

Plasma-enhanced chemical vapor deposition (PECVD) from silane (or disilane) is a widespread technique for fast growth of silicon films.[1] In PECVD, high deposition rates are guaranteed by the creation of reactive radicals in the gas phase. Among them, SiH_3 is believed to be the most abundant under most experimental conditions.[2,3] Since, at variance with conventional chemical vapor deposition (CVD), thermal cracking of neutral molecules at the film surface is not needed,[4–6] reactors can also operate at low temperature (T). Low-T (below 300 °C) PECVD is commonly used to grow amorphous, microcrystalline, or nanocrystalline films. At higher temperatures epitaxial films can also be obtained, provided that the ions' energy is carefully controlled so that damage is avoided. In fact, the closely related low-energy plasma-enhanced chemical vapor deposition (LEPECVD) technique, where large amount of reactants are created while keeping the kinetic energy of the impinging ions below ~15 eV, was used to grow device-quality Si or SiGe films.[7,8] Understanding the elementary processes leading to silicon growth from radicals is thus relevant for applications of amorphous thin-films and for the development of electronic and optoelectronic devices grown on crystalline Si(100) substrates.[2,4]

Unfortunately, film growth in plasma reactors is very complex both to investigate experimentally and to model at the molecular level. Information on elementary reaction steps of radicals on Si(100) has been obtained under more controlled experimental conditions.[9] Surface analysis techniques, such as secondary-ions mass spectroscopy (SIMS), temperature programmed desorption (TPD) (Refs. 10–13) and scanning tunneling microscopy (STM) (Refs. 14 and 15) have been applied to study the fate of SiH_3 radicals adsorbed on Si(100). Measurements at room temperature allow one to obtain time-resolved information on the evolution of the adsorbed species. SiH_3 radicals result from the exposure of the surface to silane (SiH_4) and disilane (Si_2H_6) at low temperature and at different partial pressures. Submonolayer coverages have been explored to investigate the behavior of nearly isolated adsorbed species on the otherwise clean surface. Silane is believed to decompose into SiH_3 and hydrogen while disilane is supposed to decompose into two adsorbed silyl radicals,[11,16] although different decomposition pathways have also been proposed for the latter.[17–19]

In a seminal paper, Gates *et al.*[10] proposed the following scenario for SiH_3 decomposition at the Si(100) surface, based on SIMS and TPD data. SiH_3 decomposes readily at 300 K according to

$$SiH_3 + db \rightarrow SiH_2 + H, \quad (1)$$

where db indicates a dangling bond belonging to a clean Si-Si surface dimer. All SiH_x species in reaction (1) and hereafter have to be considered adsorbed species if not otherwise specified. Then, at low hydrogen coverage (low silyl coverage on a nearly clean surface) SiH_2 can further decompose into adsorbed SiH and eventually into silicon adatoms according to

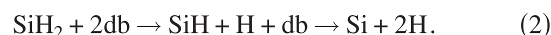

$$SiH_2 + 2db \rightarrow SiH + H + db \rightarrow Si + 2H. \quad (2)$$

At higher hydrogen coverage, when there is not a sufficient density of dangling bonds to receive hydrogen from the decomposing radicals, SiH_2 is stable: only at higher temperatures (over 200 °C) does it start diffusing on the surface, and eventually it releases hydrogen according to the recombination reaction,

$$2SiH_2 \rightarrow HSi-SiH + H_2(gas), \quad (3)$$

producing a hydrogenated dimer. Reaction (3) is responsible for the β_2 peak of H_2 release measured in TPD experiments.[10] The barrier for silyl decomposition estimated from SIMS data is very low, ranging from 80 to 100 meV, depending on silane dosage. The corresponding preexponential factors are, however, anomalously low (0.7 and 4.0 s^{-1}, respectively). It has been proposed that these low activation energies are related to processes occurring at steps and defects, at which silane precursors would preferentially adsorb. Adsorbed SiH_3 and SiH_2 species have also been identified by STM measurements at and above room temperature.[14,15] STM and SIMS agree on a lifetime of sev-

 ©2009 The American Physical Society

eral minutes for SiH_3 at room temperature. However, reaction path (2) inferred from SIMS data has been questioned by STM based on the measurement of a very precise correspondence between the number of adsorbed SiH_2 and H, which has been interpreted as resulting from the decomposition of silyl only. Moreover, no evidence of the intermediate species SiH has been detected by STM, which may be due to the very short lifetime of SiH. Nevertheless, recent TPD (Ref. 16) and modulated beam mass spectroscopy[20] measurements on Si(100) dosed with disilane are consistent with the decomposition of SiH_2 according to reaction (2).

From the theoretical side, several works are devoted to reactions leading to SiH_2 from SiH_3 in the framework of density-functional theory (DFT).[21,22] DFT slab calculations [Perdew-Burke-Ernzerhof (PBE) functional[23]] by Lim *et al.*[22] reported activation barriers of 1.12 and 1.34 eV for reaction (1), with the SiH_2 ending up in *on-dimer* and *intrarow* geometries, respectively. These activation energies are much lower than the results (2 and 2.5 eV) of Srivastava *et al.*,[24] possibly because of inaccuracies in the location of the transition state in the latter work. Earlier DFT calculations on cluster models predicted a barrier of 1.43 eV for the same reaction, the final configuration being the silylene trapped in a *broken-dimer* geometry, with the hydrogen bound to one of the Si of the broken dimer.[21] This configuration, however, is not seen in STM experiments, and the calculated barrier is incompatible with the measured lifetime of SiH_3. Other decomposition pathways of SiH_2 on the clean Si(100) surface have not been addressed yet by *ab initio* calculations. Moreover, beside possible inaccuracies due to the method used to locate the saddle point, previous theoretical works suffer from limitations stemming from the *a priori* selection of reaction pathways, a procedure which might overlook unexpected mechanisms for the reaction of the adsorbed species.

In this paper we investigate further the fate of SiH_x on Si(100), by making use of the *ab initio* metadynamics technique,[25,26] a simulation tool which allows for extensive search of diffusion and reaction pathways. As a first step toward the modeling of the growing surface, we will consider here radicals adsorbed on the clean Si(100) surface which can be compared with experimental data at low silyl (and then hydrogen) coverage. Local minima visited during (or inspired by) metadynamics trajectories have been optimized, and activation energies between different minima have been further refined by the nudged elastic band (NEB) (Ref. 27) method.

After a description of our theoretical framework in Sec. II, we present in Sec. III A the results of metadynamics simulations of an isolated SiH_3 on the clean Si(100) surface. In Sec. III B we discuss the outcome of the NEB calculations on the diffusion of silyl, on the decomposition of SiH_3 into SiH_2, on the diffusion of SiH_2 and its decomposition into SiH, and finally on the diffusion of SiH and its decomposition pathways in adatoms. In Sec. IV we report and discuss calculated STM images of relevant intermediates in comparison with experimental STM data. Section V is devoted to our conclusions.

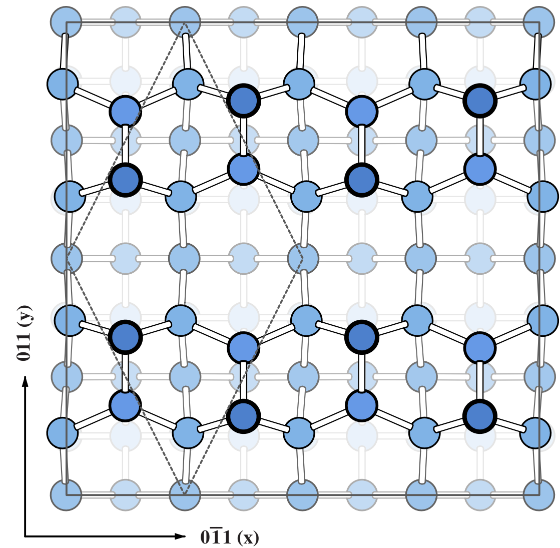

FIG. 1. (Color online) Simulation supercell adopted in this work containing eight dimers, viewed along the [100] (z) direction. The unit cell of the $c(2\times4)$ reconstruction is marked with a dashed line. Throughout this paper, the *up* atoms of the buckled dimers are highlighted with a thicker border to serve as a reference, regardless of the actual buckling state in a given geometry.

II. COMPUTATIONAL DETAILS

The calculation scheme adopted throughout this work is based on density-functional theory, using an energy functional with generalized-gradient corrections (PBE),[23] and plane-wave expansion of the Kohn-Sham orbitals up to a kinetic-energy cutoff of 25 Ry. We have used the PWSCF (Ref. 28) code for static calculations, and CPMD (Ref. 29) for Car-Parrinello[30] metadynamics simulations. Norm-conserving[31] and ultrasoft[32] pseudopotentials have been used, respectively, for silicon and hydrogen. In previous work on diffusion of SiH_3 on H:Si(100)-2×1, we have performed tests on the accuracy of our framework, by computing reaction enthalpies for some gas-phase decomposition channels of disilane.[33] As discussed in Ref. 33 and 34, spin-unrestricted calculations are mandatory to reproduce the correct reaction enthalpy of radical species. Therefore, all the calculations reported here have been performed in a spin-unrestricted framework (local spin-density approximation, LSD-PBE). The Si(100) surface is reconstructed with buckled dimers in the $c(4\times2)$ geometry. The surface is modeled by a slab, six silicon layers thick, with three-dimensional periodic boundary conditions and a vacuum gap 11 Å wide. The simulation cell contains eight surface dimers, corresponding to four $c(4\times2)$ surface unit cells (Fig. 1). The bottom surface is saturated by symmetric SiH_2 groups, which are kept fixed at the ideal bulk positions, together with the underlying silicon layer. The supercell contains a total number of 128 atoms. The theoretical equilibrium lattice parameter obtained from a bulk calculation with the k-point sampling corresponding to the supercell Γ point is 0.7% larger than the experimental one, while the theoretical value at full convergence in Brillouin-zone (BZ) integration is 0.6% shorter than the experimental one. Thus, in the slab calcula-

tion we chose the experimental lattice parameter [5.43 Å (Ref. 35)]. In previous work,[33] we found that the adsorption energy of the silyl radical on the clean Si(100)-2×1 surface (0.5 eV) changes by less than 10 meV by changing the lattice parameter by 0.7%,.

In molecular-dynamics simulations only the Γ point has been considered in the BZ sampling, whereas two special *k*-points [$(\frac{1}{4},\pm\frac{1}{4})$ in crystal coordinates] have been used in geometry optimizations and NEB calculations, as discussed later on.

We have made use of metadynamics as a tool to uncover reaction and diffusion pathways. Metadynamics allows one to overcome large barriers in a simulation time (few picoseconds) affordable in *ab initio* molecular dynamics.[25,36,37] The method is based on a coarse-grained, non-Markovian dynamics in the manifold spanned by a few reaction coordinates biased by a history-dependent potential which drives the system toward the lowest saddle point. The main assumption is that the reaction path can be described on the manifold of few collective variables (CV) $S_\alpha(\{\mathbf{R}_I\})$, which are a function of the ionic coordinates $\mathbf{R}_I$. The Lagrangian $\mathcal{L}_0$ of the system is then modified, by introducing a history-dependent biasing potential, which pushes the system out of the region it has already visited, and allows it to overcome the lowest energy barrier and move toward a new equilibrium basin. Many variations over these basic principles have been explored; in this paper we use the direct metadynamics approach,[37] which simply introduces a repulsive potential $\{\mathcal{L}=\mathcal{L}_0-g[(\mathbf{R}_I),t]\}$ built from the superposition of Gaussians centered at points previously visited by the trajectory in CV space, which acts directly on the ionic coordinates $\mathbf{R}_I$ as

$$g[(\mathbf{R}_I),t]=w\sum_{t_j<t}\exp\left[-\frac{\sum_{\alpha=1}^{n}\{S_\alpha[\mathbf{R}_I(t)]-S_\alpha[\mathbf{R}_I(t_j)]\}^2}{2\Delta s^2}\right]. \quad (4)$$

The height w and width Δs of the Gaussians are chosen in such a way as to uniformly fill the free-energy wells. We have performed metadynamics simulations of diffusion and decomposition of a single silyl and a single SiH on the clean surface. To this aim, we have chosen in both cases the (x,y) surface position of the silicon atom of the radical to be used as collective variables. This choice for the collective variables is clearly well suited to the study of diffusion, and it turned out to be sufficient to study decomposition reactions as well, since diffusion and decomposition are competitive processes, with similar activation barriers. The underlying *ab initio* dynamics is based on the Car-Parrinello method[30] with a time-step of 6 a.u., an electron fictitious mass of 600 a.u., and deuterium mass for hydrogen. We have used norm-conserving[31] pseudopotentials and a plane-waves cutoff of 18 Ry, as these simulations are only aimed at a preliminary exploration of the potential-energy surface. Constant temperature (300 K) on ions is enforced by a Nosé-Hoover thermostat.[38,39] The hills parameters [Eq. (4)] are chosen as Δs=0.26 Å and w=0.22 eV; a new hill is added each time the trajectory reaches a point $2\Delta s$ far from the previous Gaussian centers in CV space, or at worst every 300 time steps. In principle, metadynamics allows one to compute activation free energies from a finite temperature simulation. However, long simulations with a small Gaussian height w are needed to obtain accurate estimates of activation free energies. Once we have obtained a good starting guess for the transformation path out of the metadynamics trajectory, the geometry and activation energy of the transition state have been further refined by optimizing the minimum energy path (MEP) with the NEB method.[27] Climbing image and variable springs[40] have been used, with k_{max}=0.6 a.u. and k_{min}=0.3 a.u. A minimization scheme has been applied until the residual total forces acting on each image in the direction perpendicular to the path were less than 0.05 eV/Å.

In previous work on the diffusion of SiH_3 on hydrogenated Si(100) it turned out that good accuracy is obtained by performing geometry optimizations of minima and transitions states (TS) with Γ point-only sampling of the Brillouin zone, followed by a self-consistent energy calculation using a special k point.[33] This is also true for most of the configurations studied in the present work. However, for a few ones where diradical electronic states are present, Γ-only and multiple k-points calculations result in qualitatively different electronic configurations, and the error on energy differences due to the use of Γ-optimized geometries is as high as 0.3 eV. A more thorough discussion of this rather technical issue is deferred to the supplementary materials.[41] Although only a few configurations suffered from this problem, for the sake of consistency all the local minima and TS geometries have been fully optimized using the aforementioned two special k points. To speed up the optimization of TS geometries, we have applied the dimer method,[42] starting from the saddle-point geometry and the tangent to the reaction path as obtained from Γ-only NEB calculations.

III. RESULTS

A. Preliminary metadynamics simulations

The starting geometry for our metadynamics simulation corresponds to a SiH_3 radical adsorbed on a dangling bond of a surface dimer (panel A in Fig. 2). An SiH_3 radical impinging on the clean Si(100) surface would bind to a surface dangling bond with a nearly unitary sticking coefficient as demonstrated by previous theoretical investigation.[3] As discussed in Sec. II, we used as collective variables the (x,y) coordinates which locate the position of the Si atom of the adsorbed radical.

We observed a few hops of the SiH_3 radicals among the two dangling bonds of the dimer on which it was initially adsorbed, but once the added Gaussians pushed the silyl away from the dimer, instead of hopping onto the adjacent dimer, the SiH_3 decomposed into SiH_2 and H, as shown in Fig. 2(C). This outcome suggests that decomposition into silylene is more favorable than diffusion. Subsequently, the *intradimer* SiH_2 is forced to jump in the nearby location [Fig. 2(D)]. Then, instead of further diffusing away under the action of the history-dependent potential, the silylene decomposed into SiH, as shown in panel E, finally reaching a trap state (which will be discussed below). The whole trajectory

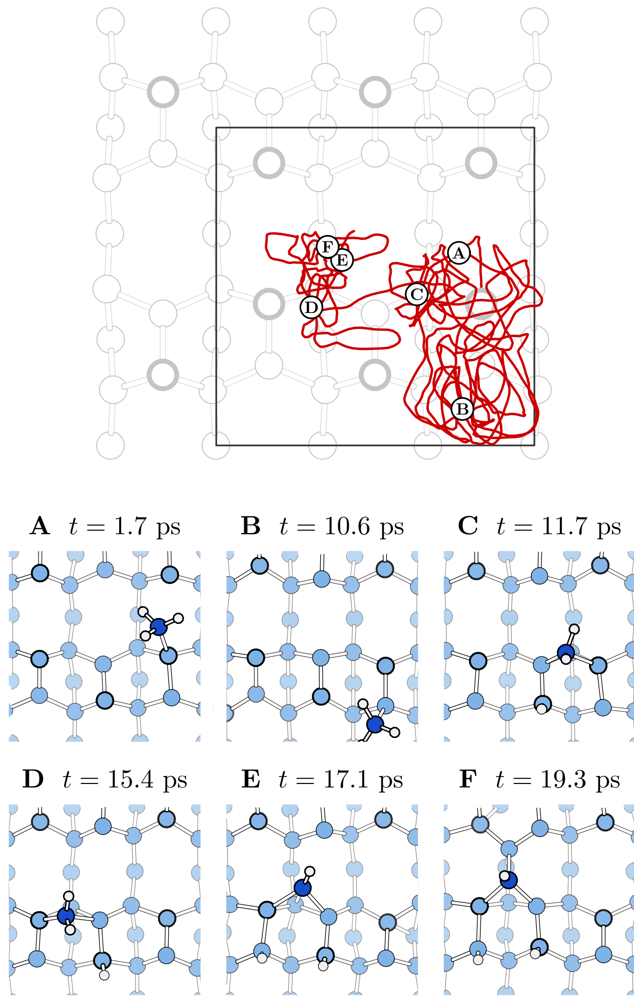

FIG. 2. (Color online) Trajectory of the (x, y) coordinates of the silicon atom of the silyl during the metadynamics simulation, superimposed to our simulation box. A series of snapshots taken along the trajectory are reported below. Only the relevant part of the box, highlighted with a thick line, is drawn. Along the path one witnesses the intradimer diffusion, the decomposition into SiH_2 and eventually into SiH; a movie of the complete trajectory is available as additional material (Ref. 41).

lasts 20 ps. A sketch of the full trajectory in CV space is shown in the upper panel of Fig. 2.

The $SiH_2 \rightarrow SiH + H$ pathway is interesting, since it seems to have an activation energy comparable or lower than the barrier for SiH_2 diffusion. These results support the predominance of reaction path (2), as inferred from earlier SIMS and TPD measurements[10] and by later experiments.[16]

To reliably assess the predominance of one reaction channel over the many others conceivable, we have undertaken extensive NEB calculations to assign activation and reaction energies among local minima identified in the metadynamics run, and several others starting from an adsorbed SiH_2 or SiH from an otherwise clean surface. Additional minima and transformation paths previously proposed in literature have also been considered. Furthermore, we also explored pathways that seemed likely to be viable in the light of the behavior observed in the metadynamics simulations. The outcome of the NEB calculations is discussed in Sec. III B. To simplify the discussion, we introduce here a notation to classify the very many configurations we are going to consider later on. Since all configurations correspond to a clean Si(100) surface plus one additional silicon atom and a variable number of hydrogen atoms, we will label local minima according to the scheme $\mathbf{N}_{\alpha}^{m}$, where $\mathbf{N}$ indicates the total number of H atoms present, m is the number of hydrogen atoms which are bound to the adsorbed silicon atom, and α is a label to distinguish configurations with identical $\mathbf{N}$ and m. For instance, the local minima corresponding to configurations in Fig. 2, panels A, C, and F will be labeled in the following as $\mathbf{3}_{a}^{3}$, $\mathbf{3}_{a}^{2}$, and $\mathbf{3}_{e}^{1}$ respectively. Configurations $\mathbf{N}_{\alpha}^{m}$ and $\mathbf{N}_{\alpha'}^{m}$ differ only because of the buckling state of nearby dimers. Configurations $\mathbf{N}_{\alpha}^{m}$ and $\mathbf{N}_{\bar{\alpha}}^{m}$ have the same energy and they can be converted one into the other by a symmetry operation.

B. Local minima and activation energies

Energies (eV) of local minima and transition states are reported in four synoptic figures (Figs. 3–5 and 8). A reference state is chosen for each figure, and its energy is set to zero. Absolute energies can be compared within the same figure, but not between different ones. Activation barriers can be obtained as a difference in energy between the transition and initial states. For a few, selected reaction pathways we have computed harmonic vibrational frequencies ν by finite displacements of the atoms (Γ-only calculations) and obtained zero-point energy (ZPE) corrections, and the prefactors $\nu^{\star}$ for reaction rates within harmonic transition state theory. In the classical limit, $\nu^{\star}=\Pi_j \nu_j^{(R)}/\Pi_j \nu_j^{(TS)}$ where $\nu_j^{(R)}$ and $\nu_j^{(TS)}$ are the positive eigenvalues of the Hessian matrix for reactant and transition states, respectively. Reaction rates and ZPE corrected energies are reported in the synoptic figures, when available, together with the energies without ZPE corrections.

At room temperature the flipping of the buckled dimers is very fast, its barrier being around 0.1 eV.[43] Therefore, only in few cases have we considered pathways differing only by the buckling of dimers on which the different species are adsorbed. In all the cases considered, the resulting difference in energy is below 0.1 eV. The synoptic figures contain all the information about decomposition pathways that emerged from the *ab initio* calculations. In brief, Fig. 3 reports diffusion and decomposition pathways for an adsorbed SiH_3, and also considers further decomposition events which ultimately lead to an adsorbed silicon adatom. Figure 4 displays similar processes in the presence of an additional adsorbed H. Figure 5 collects the diffusion and decomposition pathways of an isolated SiH_2, which might be produced by the intermediate silylene diffusing away from the initial adsorption site of the silyl. Finally, Fig. 8 displays diffusion and decomposition pathways of an isolated SiH, which we found to be an intermediate step in our decomposition pathways, and which received scarce attention so far. The reader can refer to Fig. 3 for all structures of the form $\mathbf{3}_{\alpha}^{m}$, to Fig. 4 for $\mathbf{4}_{\alpha}^{m}$, to Fig. 5 for $\mathbf{2}_{\alpha}^{m}$, and to Fig. 8 for $\mathbf{1}_{\alpha}^{m}$ minima.

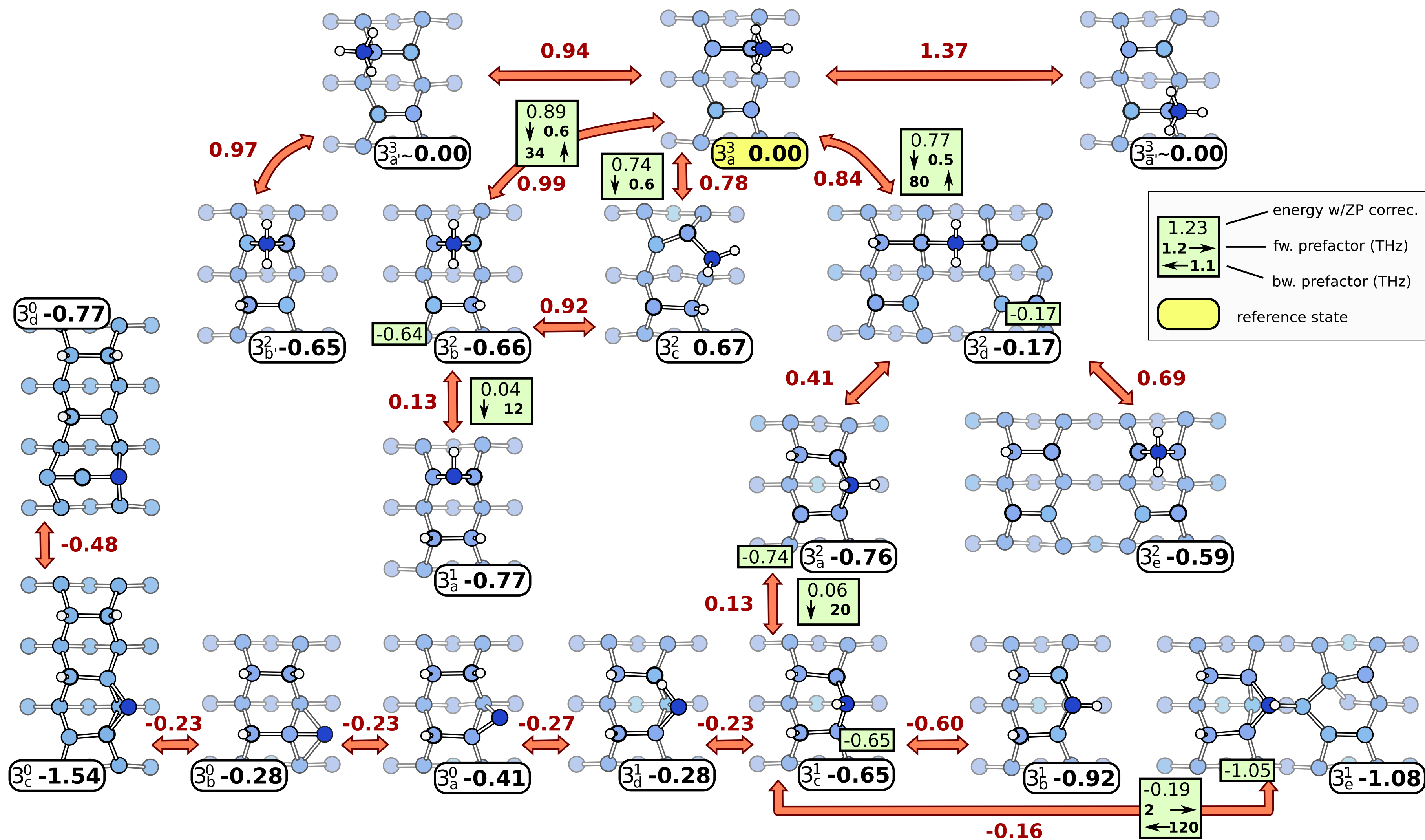

FIG. 3. (Color online) Synoptic scheme of the diffusion and decomposition pathways of SiH_3 on the clean Si(100) surface. The different configurations are labeled as $\mathbf{3}^m_\alpha$ where the number indicates that there are three H atoms of which m are bound to the silicon adatom; α labels different configurations with the same m. Configurations $\mathbf{3}^m_\alpha$ and $\mathbf{3}^m_{\alpha'}$ differ only because of the buckling state of the dimers. Energies (eV) with respect to a reference state ($\mathbf{3}^3_a$) are given for the local minima in rounded boxes. Energies of the transition states (with the same zero energy reference) are given above the arrows connecting two local minima. Energies corrected by ZPE and frequency prefactor (terahertz) in reaction rates (see text) are given in squared boxes for selected local minima and reactions. The reference of energy is again the state ($\mathbf{3}^3_a$) also with ZPE correction. Reaction energies are obtained as energy difference between the local minima, while activation energies for reactions are obtained as energy differences of transition and initial state.

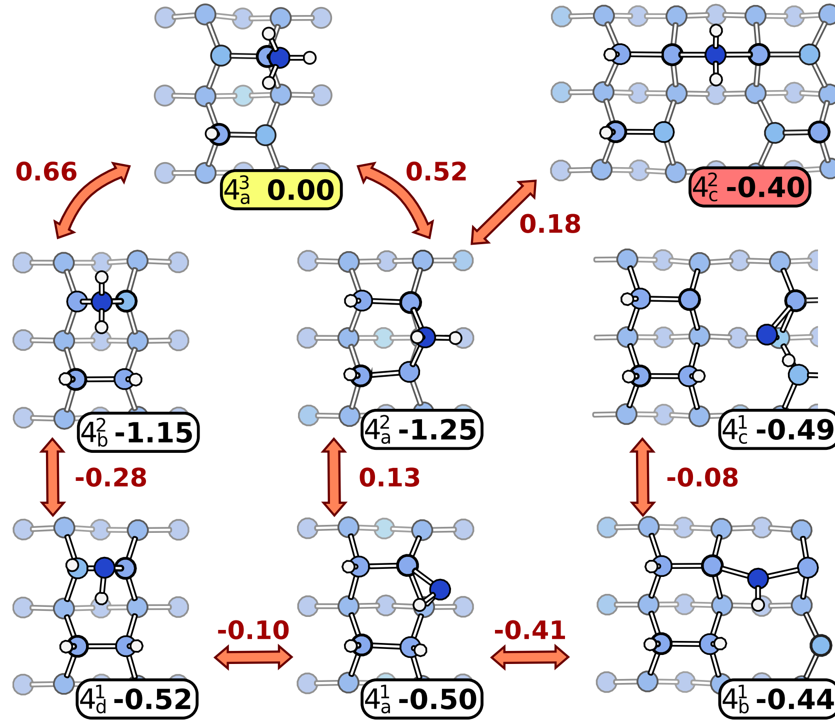

FIG. 4. (Color online) Synoptic scheme of decomposition pathways of SiH_3 in the presence of an additional adsorbed H atom. The different configurations are labeled as $\mathbf{4}^m_\alpha$ where the number indicates that there are four H atoms of which m are bound to the silicon adatom; α labels different configurations with the same m. Energies (eV) of local minima and transition states are given. For all other notations see caption of Fig. 3. All the configurations are in a closed-shell state, but for $\mathbf{4}^2_c$ which is a diradical.

1. Diffusion and decomposition of SiH_3

In its most stable adsorption configuration, SiH_3 (Refs. 44 and 45) is bound to one of the silicon atoms of a surface dimer (structure $\mathbf{3}^3_a$). The difference in energy that results from the buckling of nearby dimers is less than 10 meV, and the activation energy for jumping between the two atoms of the same dimer is 0.94 eV ($\mathbf{3}^3_a \to \mathbf{3}^3_{a'}$). To diffuse along the dimer row ($\mathbf{3}^3_a \to \mathbf{3}^3_{\bar{a}'}$) a barrier of 1.37 eV must be overcome. Diffusion of silyl is pre-empted by decomposition ($SiH_3 \to SiH_2 + H$), through competitive channels with barriers in the 0.8–1.0 eV range, i.e., pathways $\mathbf{3}^3_a \to \mathbf{3}^2_b$, $\mathbf{3}^3_a \to \mathbf{3}^2_c \to \mathbf{3}^2_b$, $\mathbf{3}^3_a \to \mathbf{3}^2_d \to \mathbf{3}^2_a$ (cf. Fig. 3). The intrarow configuration of SiH_2 in the presence of the extra H atom ($\mathbf{3}^2_a$), is 0.10 eV more stable than the on-dimer structure ($\mathbf{3}^2_b$), in agreement with previous theoretical results.[46] Conversely, on the clean surface the relative stability of the corresponding configurations ($\mathbf{2}^2_b$ and $\mathbf{2}^2_a$ in Fig. 5) is reversed, the on dimer being 0.17 eV more stable than the intrarow.[47,48] The lowest energy barrier we found is 0.84 eV, for the $\mathbf{3}^3_a \to \mathbf{3}^2_d$ reaction, which is further lowered to 0.77 eV when ZPE corrections are taken into account. The intermediate state $\mathbf{3}^2_d$ can then evolve to the more stable $\mathbf{3}^2_a$ or $\mathbf{3}^2_e$ structures.

We can estimate the average lifetime τ of an SiH_3 within transition state theory, $\tau^{-1} = \nu^\star \exp(-\Delta E / k_B T)$, by choosing for the activation energy and frequency prefactor the calculated values $\Delta E = 0.8$ eV and $\nu^\star = 0.5$ THz (cf. Fig. 3). The resulting lifetime is ~ 48 s, which is compatible with the lifetime of few minutes measured by STM (Refs. 14 and 15) and SIMS.[10] Although theoretical and experimental lifetimes are similar, barriers and prefactors computed from SIMS data are anomalously low (~ 0.1 eV and ~ 1 Hz, respectively). It has been proposed that the low activation energy for decomposition might be related to preferential adsorption of silane at surface defects.[15] Moreover, activation energy measured from SIMS data seems to depend on the type of precursor (0.1 eV for SiH_4, and 0.27 eV for disilane[10]). That said, STM measurements report similar decomposition rates due to processes occurring on a flat, defectless surface. Our results suggest that decomposition of SiH_3 can indeed take place on a clean terrace, with a lifetime on the order of minutes, and with prefactors compatible with the values generally observed for similar simple surface reactions. The activation energies for decomposition according to the $\mathbf{3}^3_a \to \mathbf{3}^2_a$ and $\mathbf{3}^3_a \to \mathbf{3}^2_b$ pathways had previously been computed within a similar DFT framework by Lim *et al.*,[22] who found the values 1.12 and 1.34 eV, respectively, as opposed to our values of 0.84 and 0.99 eV. An overestimation of the activation barriers is expected due to the use of a scheme for MEP optimization which is less reliable than the NEB method used here. Actually, the intermediate state $\mathbf{3}^3_d$ along the $\mathbf{3}^3_a \to \mathbf{3}^2_a$ decomposition channel is not found in Ref. 22.

In short, our results support the picture in which SiH_3 does not diffuse on the clean surface, but readily decomposes into SiH_2 at room temperature.

2. Decomposition of SiH_2

SiH_2 is not stable in configurations $\mathbf{3}^2_b$ and $\mathbf{3}^2_a$ as the barrier for decomposition according to $SiH_2 \to SiH + H$, via one of

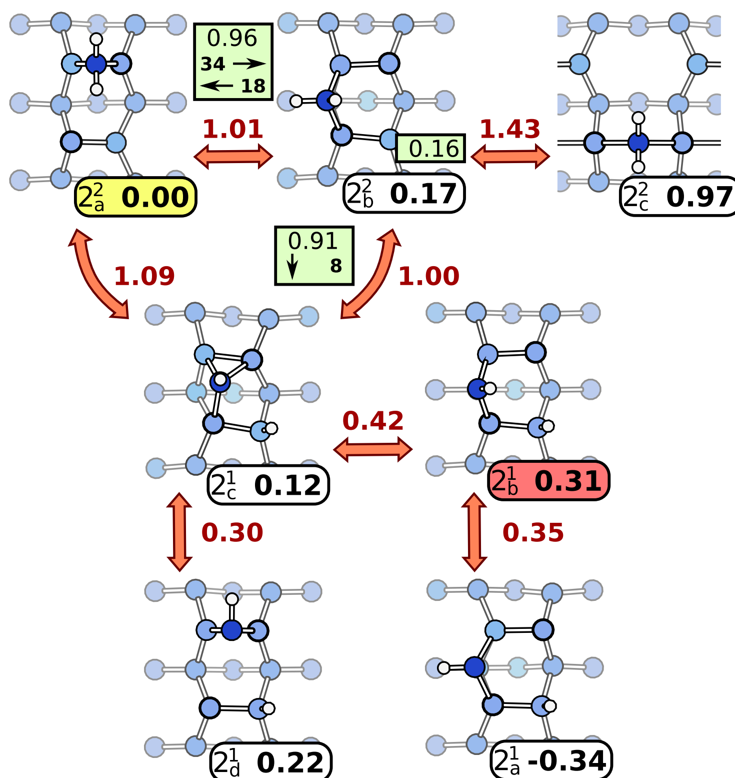

FIG. 5. (Color online) Synoptic scheme of the diffusion and decomposition pathways of SiH_2 on the clean Si(100) surface. The different configurations are labeled as $\mathbf{2}_{\alpha}^{m}$ where the number indicates that there are two H atoms of which m are bound to the silicon adatom; α labels different configurations with the same m. Energies (eV) of local minima and transition states are given. For all other notations see caption of Fig. 3. All the configurations are in a closed-shell state, but for $\mathbf{2}_{b}^{1}$ which is a diradical.

the channels $\mathbf{3}_{b}^{2}\rightarrow\mathbf{3}_{a}^{1}$, $\mathbf{3}_{a}^{2}\rightarrow\mathbf{3}_{c}^{1}\rightarrow\mathbf{3}_{b}^{1}$, or $\mathbf{3}_{a}^{2}\rightarrow\mathbf{3}_{c}^{1}\rightarrow\mathbf{3}_{e}^{1}$, is comparable to the barrier for decomposition of SiH_3 into SiH_2. This further decomposition step is facilitated by the presence of the additional hydrogen atom bound to the nearby dimer. In the absence of this additional H atom, the activation energies rise to 1.0 eV along the pathways $\mathbf{2}_{a}^{2}\rightarrow\mathbf{2}_{c}^{1}$ and $\mathbf{2}_{a}^{2}\rightarrow\mathbf{2}_{b}^{2}\rightarrow\mathbf{2}_{c}^{1}$ (cf. Fig. 5). The resulting adsorbed SiH can then reach the trap state $\mathbf{2}_{a}^{1}$ or diffuse away overcoming small barriers via channels that we will discuss in detail later on. For an isolated SiH_2 on the clean surface, decomposition into SiH is in competition with diffusion along the dimer rows. The activation energy for diffusion along the row ($\mathbf{2}_{a}^{2}\rightarrow\mathbf{2}_{b}^{2}$) is actually 1.01 eV. Diffusion of SiH_2 to adjacent dimer rows involves overcoming the much larger barrier of 1.43 eV ($\mathbf{2}_{a}^{2}\rightarrow\mathbf{2}_{b}^{2}\rightarrow\mathbf{2}_{c}^{2}$). In the search for the lowest energy diffusion pathways of SiH_2 we have explored all the transitions between the local minima identified in Ref. 48. Therefore, in-row diffusion and decomposition into SiH are competing processes on the clean surface.

As suggested by the metadynamics simulations, the calculated lifetimes of SiH_3 and of SiH_2 are similar [respectively, 48 s for SiH_3, 6 min for SiH_2 on the clean surface ($\mathbf{2}_{a}^{2}\rightarrow\mathbf{2}_{b}^{2}\rightarrow\mathbf{2}_{c}^{1}$) and 3 s in presence of a hydrogen atom ($\mathbf{3}_{a}^{2}\rightarrow\mathbf{3}_{c}^{1}$)]. However, we cannot draw compelling conclusions on the predominance of decomposition of SiH_2 with respect to diffusion because of insufficient accuracy in the calculated activation energies. Errors of the order of 0.1 eV in the activation energies are expected due to overall inaccuracies of the DFT-GGA framework. With this fundamental accuracy issue in mind, we can move on to a consideration of how our results fit to the experimental data. The scenario which fits best our findings is the stepwise decomposition of SiH_2 down to adatoms according to reaction (2). The decomposition of SiH into adatoms is as fast as the previous two steps, as will be discussed later on. However, some problems arise with respect to the interpretation of STM data.[14,15] Namely,

(i) If SiH_2 is not stable at room temperature, what is the configuration which is assigned to an intrarow silylene, immobile at 300 K?

(ii) If SiH_2 readily decomposes into SiH, why has no signal been detected in STM which can be assigned to this latter species?

(iii) Is the picture emerging from simulations compatible with the β_2 release of H_2 at higher temperature and at higher coverage?

Regarding question (i) above, a possible explanation is that the decomposition of SiH_2 is hindered by the presence of additional hydrogen atoms at the surface, which is very likely at high SiH_3 coverage. Consider for instance the scenario shown in Fig. 4. A silyl radical adsorbed on a dimer with a nearby hemihydrogenated dimer can decompose into SiH_2 with a barrier as low as ~0.5 eV ($\mathbf{4}_{a}^{3}\rightarrow\mathbf{4}_{a}^{2}$). Not only is the intrarow configuration more stable than the on dimer, but the former ($\mathbf{4}_{a}^{2}$) is a deep trap state for the silylene, which cannot decompose nor diffuse at room temperature, the barrier for escape being ~1.4 eV. Problem (ii) can be solved by considering that SiH is both short lived and diffuses too

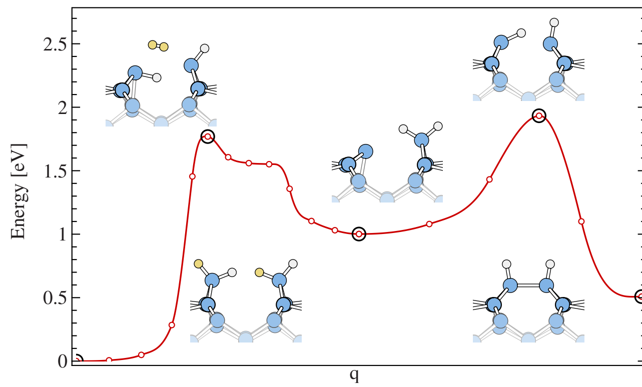

FIG. 6. (Color online) Energy profile along the minimum-energy path for β_2 reaction of two SiH_2 groups, followed by the formation of a NRMH dimer. The structures of local minima and transition states are also sketched.

quickly to be detected in a fixed configuration by STM measurements as we will discuss below.

Concerning question (iii) on the H_2 release observed at high temperature [$\sim$650 K (Ref. 10)], we recall that the β_2 peak in TPD, assigned to reaction (3), is observed at high coverage (high dose of silane or disilane precursor). Under these conditions the hydrogen coverage is expected to be high and the fully hydrogenated SiH_2 intrarow configuration ($\mathbf{4}_a^2$) might be seen as a silicon adatom on a (locally) hydrogenated Si(100)-2$\times$1 surface. It is known[49,50] that such an adatom can diffuse along the rows with an activation energy of 1.4 eV, which would corresponds to a diffusion of silylene via concerted hydrogens exchange. Once two SiH_2 meet in configuration $\mathbf{4}_a^2$, they could give rise to the β_2-H_2 release observed in Ref. 10. Such a channel for silylene diffusion on fully hydrogenated surface would be viable at temperatures high enough for the experimental β_2 activation barrier (1.87 eV) (Ref. 51) to be overcome. Two theoretical estimates are available at present for the barrier to this reaction. The first is lower than the experimental value [1.45 eV (Ref. 52)], which is probably due to the use of the simple DFT-LDA functional which usually underestimates activation energies. The second [2.32 eV (Ref. 21)] is higher, and corresponds to a different process, which involves two on-dimer SiH_2, and results in a different configuration than the experimentally observed nonrotated monohydrogenated (NRMH) dimer.[52] We therefore decided to repeat the calculations, combining a preliminary metadynamics run with NEB static optimization of the reaction path. The final result is reported in Fig. 6, and provides interesting insights, which aid in explaining problems (i) and (iii). The barrier for H_2 release is 1.76 eV, in excellent agreement with experimental data, although the barrier might be slightly different on the hydrogenated surface. The transition state is stabilized by the presence of a hydride "bridging" between the two Si atoms. In fact, the barrier for the reaction occurring without SiH_2 tilting, which results in the reaction of the two central hydrogens, is 0.5 eV higher. Similar behavior is observed in Ref. 21 where the activation energy for the reaction between the two central hydrogens is much higher than a concerted reaction ending up with a "bridged" configuration (although for on-dimer

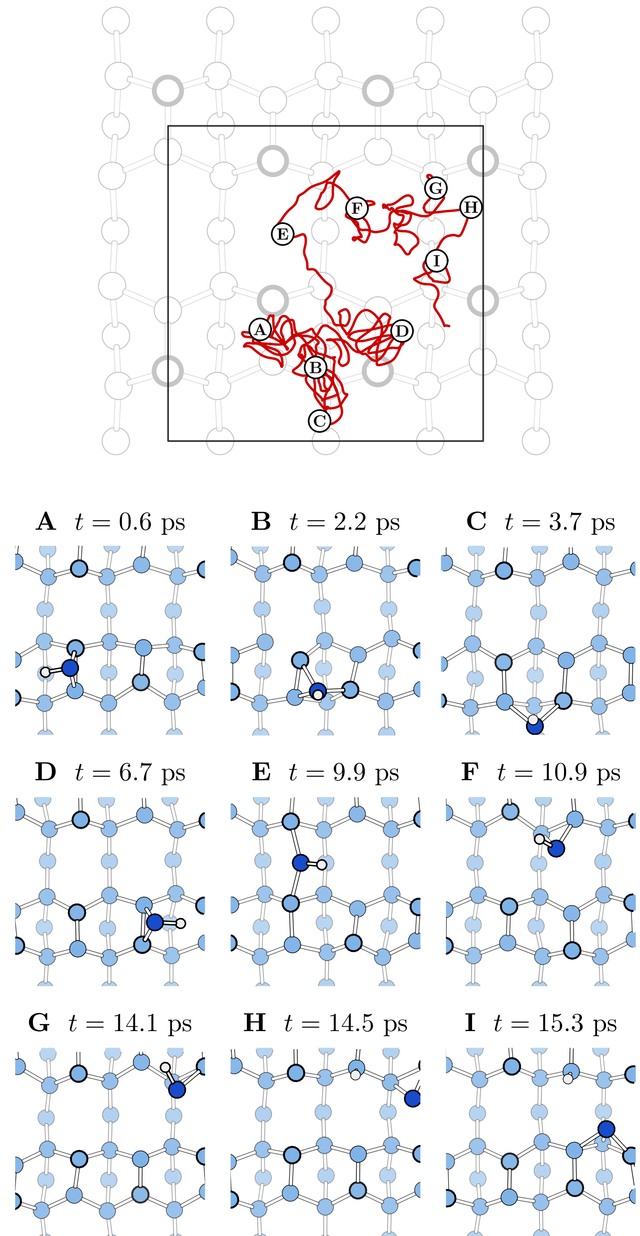

FIG. 7. (Color online) Trajectory of the (x,y) coordinates of the SiH silicon atom during the metadynamics simulation. A series of snapshots taken along the trajectory are reported below; only the relevant part of the simulation box is drawn. A movie of the complete trajectory is available as additional material (Ref. 41).

SiH_2). The reaction between the two SiH_2 in Fig. 6 does not result in the immediate formation of a NRMH dimer, but produces an adatom and SiH_2 pair. The further reaction to form the NRMH dimer has a barrier of 0.93 eV. However, we cannot exclude that kinetic effects beyond transition state theory applied here could drive the system directly toward the NRMH product skipping the intermediate local minimum. Nevertheless, our finding actually provides additional insight to explain the experimental STM results. In fact, on the hydrogenated surface the two fragments may react to give a NRMH dimer, but on the clean surface the barrier for diffusion of the adatom is only $\sim$0.6 eV, and the Si might

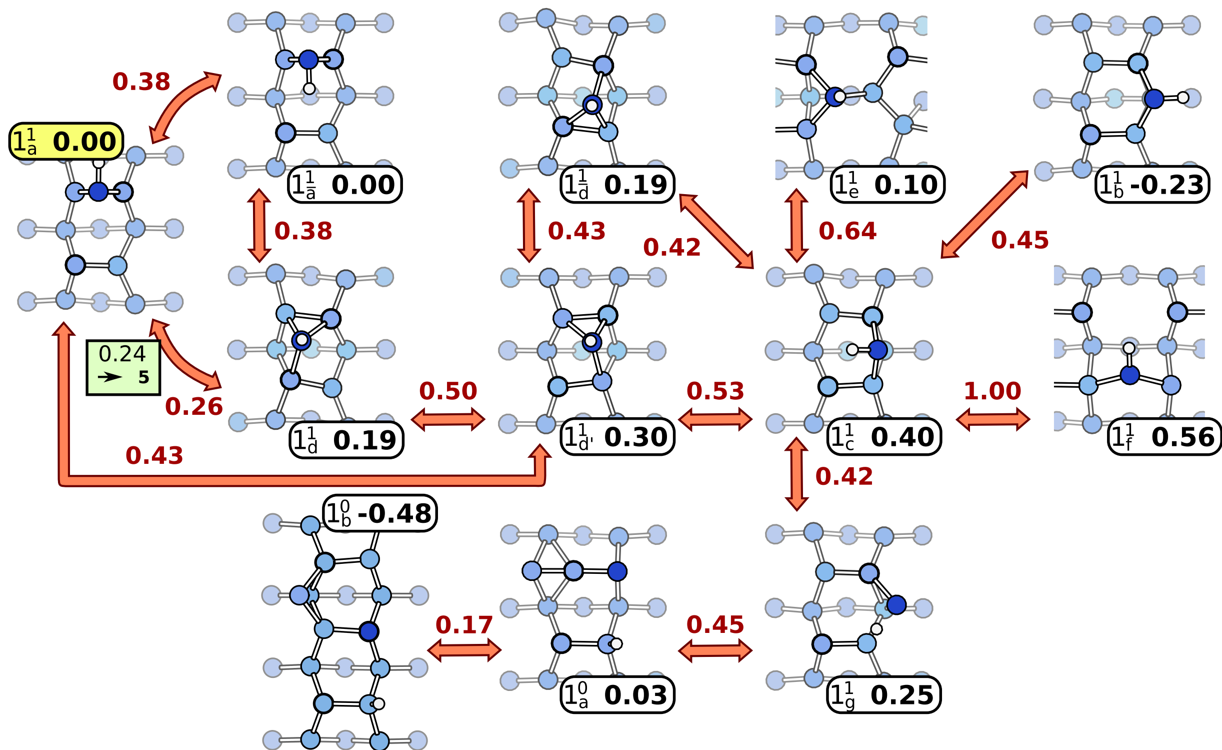

FIG. 8. (Color online) Synoptic scheme of the diffusion and decomposition pathways of SiH on the clean Si(100) surface. The different configurations are labeled as $\mathbf{1}^m_\alpha$ where the number indicates that there is one H atom bound ($m=1$) or unbound ($m=0$) to the silicon adatom; α labels different configurations with the same m. Energies (eV) of local minima and transition states are given. For all other notations see caption of Fig. 3.

diffuse away before reacting. Then we speculate that NRMH dimers observed by STM at low coverage might not be the direct result of β_2 reaction of two SiH_2, but of the reaction of an SiH_2 trapped in configuration $\mathbf{4}^2_a$ and of an adatom wandering along the adjacent dimer row, produced from the complete dehydrogenation of another radical (see also Sec. III B 3). Moreover, we found that two nearby SiH_2 are 0.16 eV higher in energy than when far away from each other. This is easy to understand in terms of steric hindrance between the hydrides. Even at 450 K, simple statistical considerations suggest that the probability of finding one such a pair is as low as 1%, which is lowered further if one takes into account configurational entropy at low coverage. This scenario also fits better the evidence of NRMH formation at 470 K, a temperature sizably lower than the TPD peak at 670 K assigned to the β_2 process (with an experimental activation energy of 1.87 eV). The β_2 reaction of Fig. 6 still takes place at high coverage when adatoms diffuse on the hydrogenated surface as discussed previously.

In short, our calculations suggest that the picture of a SiH_2 diffusing intact on the surface at low coverage must be revised, because the lifetime of silylene is similar to that of SiH_3 due to decomposition into SiH and then into Si and H (see Sec. III B 3). On the clean surface competitive channels exist for SiH_2 diffusion and decomposition, but SiH_2 is stable at room temperature once bound to two hemihydrated dimers. This latter configuration might arise from the decomposition of the silyl radical in the presence of a hemihydrated dimer.

3. Diffusion and decomposition of SiH

In order to achieve a better understanding of the behavior of a SiH radical on the clean surface we have performed an in-depth analysis. First, we have performed a metadynamics run starting from the on-dimer configuration ($\mathbf{1}^1_a$, cf. panel A of Fig. 7), and using the collective variables and parameters we used for SiH_3 (cf. Sec. II). In the time span of 16 ps, the SiH group diffuses along the dimer row (panels A–D), jumps onto the adjacent row (panels E–G) and eventually decomposes into an adsorbed hydrogen and a Si adatom. The trajectory in CV space is sketched in the upper panel of Fig. 7. Local minima observed along the trajectories and few others are reported in Fig. 8. The diffusion of SiH along the dimer row takes place via the path $\mathbf{1}^1_a \rightarrow \mathbf{1}^1_{d'} \rightarrow \mathbf{1}^1_{\bar{d}} \rightarrow \mathbf{1}^1_{\bar{a}}$ with an overall barrier of 0.43 eV. To diffuse to an adjacent row the

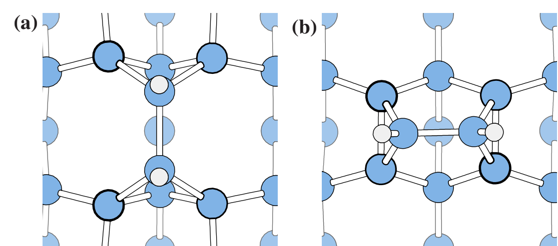

FIG. 9. (Color online) Hydrogenated dimers obtained by barrierless reaction of two SiH fragments: (a) an "on-channel" dimer, obtained from $\mathbf{1}^1_c$ configuration, and b) an "on-row" dimer, obtained from $\mathbf{1}^1_a$ configuration.

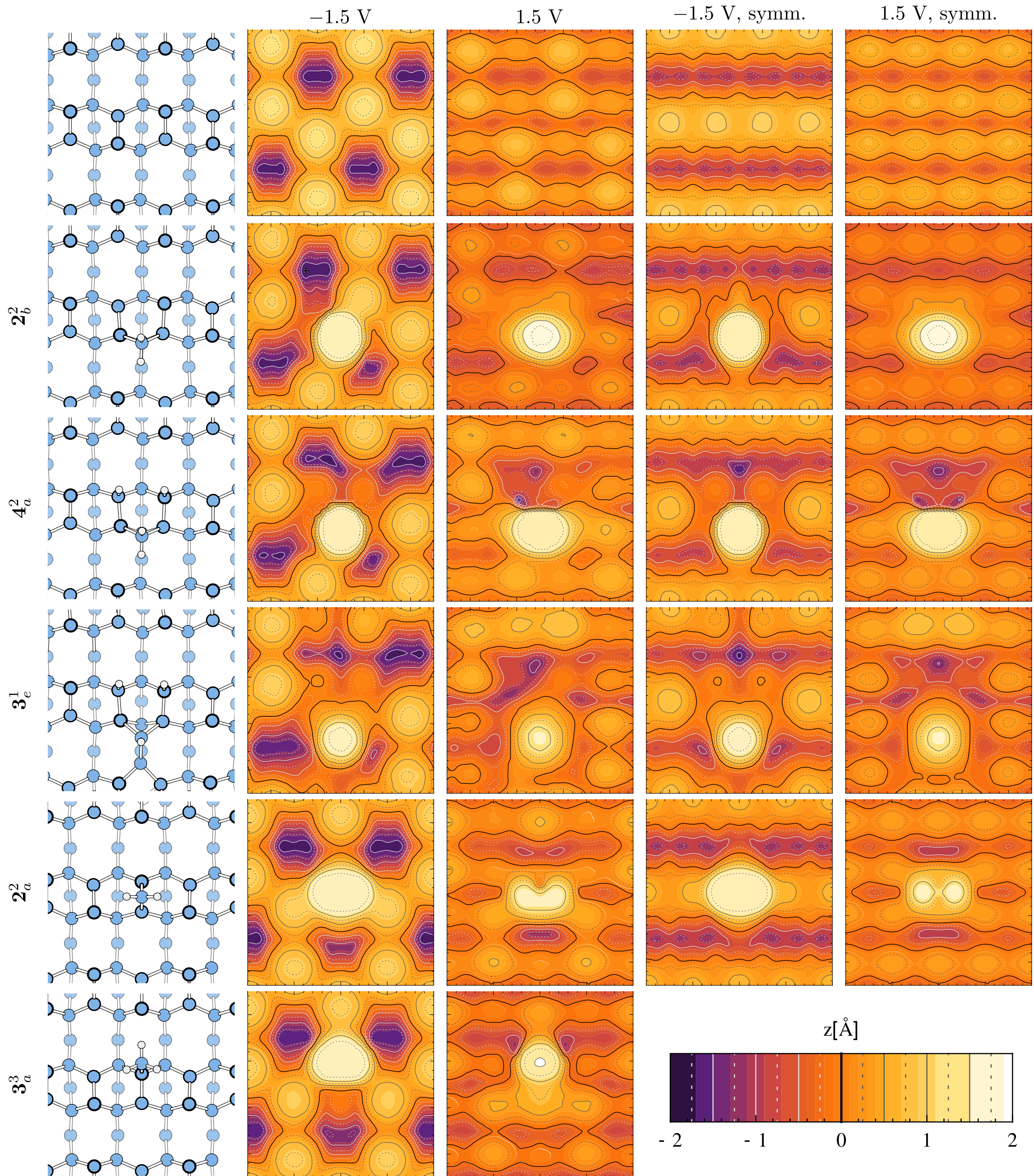

FIG. 10. (Color online) Simulated STM images of different metastable minima for SiH_x radicals on Si(100) surface. Plots represent height profiles of the surface at a constant local density of states (0.8×10^{-5} a.u.), for −1.5 V (filled states) and 1.5 V (empty states) tip-sample biases. In the Tersoff-Hamann approximation, the plot corresponds to a constant-current image. All the structures but $\mathbf{3}_a^3$ exist in two symmetry-equivalent buckling states. The first two profiles correspond to frozen dimers, while in the last two we plot the average of the two equivalent configurations, which takes into account to a certain extent the dynamic average of the STM images to be expected in a room-temperature measurement. The profile for the clean surface is plotted as a reference, and the average height for the clean surface for each bias is taken as the zero height for the other images.

activation barrier is instead as high as 1 eV (via $\mathbf{1}_c^1 \rightarrow \mathbf{1}_f^1$). From configuration $\mathbf{1}_{d'}^1$, SiH can move to the (shallow) trap state $\mathbf{1}_b^1$ or decompose into Si and H adatoms (via $\mathbf{1}_{d'}^1 \rightarrow \mathbf{1}_c^1 \rightarrow \mathbf{1}_g^1 \rightarrow \mathbf{1}_a^0 \rightarrow \mathbf{1}_b^0$) with an activation energy of 0.45 eV. By using a frequency prefactor of 0.5 THz and an activation energy of 0.43 eV, we obtain a jump rate at room temperature of 33 kHz which is too high for SiH to be seen in STM, at least in 1994 when the latest measurements on this system have been made.[15] Therefore, either SiH moves or decomposes too fast on the clean surface to be detected by STM. However, we have also identified a trap state for SiH in the presence of additional H atoms. In fact, in configuration $\mathbf{3}_e^1$ produced by a stepwise decomposition [reactions (1) and (2)], detrapping of SiH and decomposition into adatoms requires overcoming an activation barrier of 0.92 eV (via $\mathbf{3}_e^1 \rightarrow \mathbf{3}_c^1 \rightarrow \mathbf{3}_d^1 \rightarrow \ldots \rightarrow \mathbf{3}_d^0$). This trap state for SiH is expected to be as long lived as the SiH_3 and SiH_2 precursors on the clean surface (i.e., with a life time of minutes). Structures $\mathbf{3}_e^1$ and $\mathbf{4}_a^2$ both have the correct symmetry to produce an STM image similar to that recorded in experiments and assigned to an SiH_2 group, as we will discuss in more detail in Sec. IV.

We would also like to mention that SiH diffusion offers another scenario for the formation of monohydride dimers (H-Si-Si-H) at room temperature. As shown in Fig. 9 two SiH can react in configuration $\mathbf{1}_c^1$ on adjacent dimer rows, giving rise to a NRMH dimer, or in configuration $\mathbf{1}_a^1$ on the same row, the "on-row" configuration being ~0.9 eV more stable than the "on-channel" one. Both reaction pathways are barrierless.

At low H coverage the decomposition of SiH_3 down to mobile silicon adatom and adsorbed hydrogen would also lead to the formation of Si-Si ad-dimers, once two adatoms come close. The barriers for adatom diffusion on clean Si(100) are on the order of 0.6 eV along the dimer rows, and of 1.0 eV in the perpendicular direction.[53] In this scenario, ad-dimers can form directly from adatoms, and not necessarily from hydrogenated or monohydrogenated dimers, which would be produced from the reaction of two SiH or SiH_2.

Finally we remark that all the individual decomposition reactions $SiH_3 \rightarrow SiH_2 + H$, $SiH_2 \rightarrow SiH + H$, and $SiH \rightarrow Si + H$ are exothermic. The overall energy gain in the full decomposition of the silyl into Si and H adatoms depends on the final positions of the H atoms, but it is at most of the order of 1.5 eV ($\mathbf{3}_c^0$), a value much lower than the rough estimate of 3.8 eV for the full decomposition of SiH_2 given in Ref. 10 on the basis of a bond-count argument.

IV. STM IMAGES

The adsorption geometry of SiH_3 and SiH_2 has been inferred experimentally from STM data.[14,15] SiH_3 appears as a bright spot by imaging occupied electronic states (negative bias). The STM image is consistent with the adsorption geometry $\mathbf{3}_a^3$. The adsorption geometry of SiH_2 has been assigned instead to the intradimer configuration $\mathbf{2}_b^2$ on the basis of the symmetry of the image and of the location of the protrusion detected at negative bias. However, it is not possible to discriminate between configurations $\mathbf{2}_b^2$ and $\mathbf{4}_a^2$, the latter with SiH_2 bound to hemihydrogenated dimers (cf. Figs. 5 and 4).

In Fig. 10 we report the calculated STM images for different configurations at negative (occupied states) and positive (empty states) biases. In the spirit of the Tersoff and Hamann[54] approximation, we assume the tunneling current to be proportional to the local density of states (LDOS), integrating the contributions from the states in an energy window above or below the Fermi energy as dictated by the bias potential. The images correspond to the surface topography at constant current, computed as a surface at constant LDOS. We have verified that the energy cutoff and the vacuum spacing are large enough to guarantee an exponentially decrease in the LDOS up to ~5 Å from the surface, whereas the isodensity surface we plot lies typically at ~4 Å from the underlying surface atoms.

The STM images of the configurations of SiH_2 bound to clean or hemihydrogenated dimers ($\mathbf{2}_b^2$ and $\mathbf{4}_a^2$) are indeed very similar at both positive and negative bias. Moreover, they are also similar to the STM image of the configuration of SiH bound to hemihydrogenated dimers (the trap state $\mathbf{3}_e^1$, Fig. 3). Since, as discussed in Sec. III, configuration $\mathbf{4}_a^2$ survives long enough at normal conditions, while configurations $\mathbf{2}_b^2$ and $\mathbf{3}_e^1$ do not, we propose that the geometry seen in STM is actually the former. Note that all configurations $\mathbf{2}_b^2$, $\mathbf{4}_a^2$, and $\mathbf{3}_e^1$ appear as a protrusion in the theoretical STM images at both positive and negative bias, while the experimental STM image (assigned in the experimental papers to $\mathbf{2}_b^2$) is reported in Ref. 15 (but not in the previous work[14]) to appear as a protrusion at negative voltage, but as a depression at positive voltage. The reasons for these discrepancies remain to be seen. For sake of comparison, we also report in Fig. 10 the calculated STM images of the adsorbed SiH_3, of SiH_2 in the on-dimer configuration and of the clean surface.

V. CONCLUSIONS

In summary, we have performed an extensive search for diffusion and decomposition pathways of SiH_x species on the clean Si(100) surface aiming at interpreting the experimental data on Si(100) at very low coverage. Activation energies for different reaction channels have been refined by NEB optimization of the minimum-energy paths. All the results point to the conclusion that at room temperature SiH_3 fully decomposes on the clean surface down to Si and H adatoms ($SiH_3 \rightarrow SiH_2 + H \rightarrow SiH + 2H \rightarrow Si + 3H$) in agreement with the scenario inferred from SIMS, TPD, and modulated beam mass spectroscopy data.[10,16,20] The activation energy and frequency prefactor (within harmonic transition state theory) for SiH_3 decomposition into SiH_2 are 0.8 eV and 0.5 THz, respectively, which provide a theoretical lifetime (48 s) close to experimental SIMS and STM data (few minutes). The SiH_2 product has a lifetime similar to that of SiH_3 due to decomposition into SiH. Diffusion and decomposition are competitive channels for SiH_2 on the clean surface with similar activation energy (1.0 eV). The SiH intermediate can also diffuse very fast or decompose into adatoms with activation energies sufficiently low (0.4 or 0.5 eV, respectively) to prevent its identification by STM at room temperature.

SiH_3 adsorbed nearby a hemihydrogenated dimer can decompose even faster (E_a=0.5 eV) into SiH_2 bridging two hemihydrogenated dimers. This latter species has a longer lifetime than other SiH_x configurations, the barrier for escaping or decomposing being as large as 1.4 eV. Based on calculated lifetimes and STM images, we propose that the latter species can be identified with the structure seen experimentally by STM and previously assigned to SiH_2 bridging two clean dimers.[14,15] Overall, the simulations revealed a complex scenario with very many competitive channels for diffusion and decompositions of SiH_x on the clean Si(100) surface. These results complement our previous works on the behavior of adsorbed SiH_x species at the opposite limit of a fully hydrogenated H:Si(100)-2×1 surface.[33,34,50] In order to perform a direct comparison with experiments at growth conditions, it would be necessary to investigate diffusion and decomposition channels on a partially hydrogenated surface. To this aim additional calculations may be necessary, which are left for future works. Provided with a complete database of reaction rates at intermediate H coverages, one might attempt kinetic Monte Carlo (KMC) simulations of the growing surface under PECVD conditions along the lines outlined in recent KMC simulations[55] of the fully hydrogenated surface, which is based on the *ab initio* reaction rates obtained in our previous works.[33,34,50]

ACKNOWLEDGMENTS

This work is partially supported by the Cariplo Foundation (SIMBAD project) and by European STREP Project NANOPHOTO. Computational resources have been provided by CILEA and by CINECA through CNR-INFM-CNISM "Iniziativa Calcolo Parallelo 2006." Discussions with G. Isella and C. Cavallotti are gratefully acknowledged. We thank G. Tribello for reading the paper.

---

*Present address: Computational Science, Department of Chemistry and Applied Biosciences, ETH Zürich, USI Campus, Via Giuseppe Buffi 13, CH-6900 Lugano, Switzerland; michele.ceriotti@phys.chem.ethz.ch

[1] T. J. Donahue and R. Reif, J. Appl. Phys. **57**, 2757 (1985).
[2] N. Yamauchi and R. Reif, J. Appl. Phys. **75**, 3235 (1994).
[3] S. Ramalingam, D. Maroudas, and E. S. Aydil, J. Appl. Phys. **86**, 2872 (1999).
[4] A. Matsuda, Jpn. J. Appl. Phys., Part 1 **43**, 7909 (2004).
[5] D. Maroudas, Adv. Chem. Eng. **28**, 251 (2001).
[6] C. Cavallotti, M. Di Stanislao, and S. Carrà, Prog. Cryst. Growth Charact. Mater. **48-49**, 123 (2004).
[7] C. Rosenblad, H. R. Deller, A. Dommann, T. Meyer, P. Scroeter, and H. von Känel, J. Vac. Sci. Technol. A **16**, 2785 (1998).
[8] C. Rosenblad, T. Graf, J. Stangl, Y. Zhuang, G. Bauer, J. Schulze, and H. von Känel, Thin Solid Films **336**, 89 (1998).
[9] H. Rauscher, Surf. Sci. Rep. **42**, 207 (2001).
[10] S. M. Gates, C. M. Greenlief, and D. B. Beach, J. Chem. Phys. **93**, 7493 (1990).
[11] S. M. Gates, C. M. Greenlief, D. B. Beach, and P. A. Holbert, J. Chem. Phys. **92**, 3144 (1990).
[12] S. M. Gates, C. M. Greenlief, S. K. Kulkarni, and H. H. Sawin, J. Vac. Sci. Technol. A **8**, 2965 (1990).
[13] C. M. Greenlief, S. M. Gates, and P. A. Holbert, J. Vac. Sci. Technol. A **7**, 1845 (1989).
[14] M. J. Bronikowski, Y. Wang, M. T. McEllistrem, and R. J. Hamers, Surf. Sci. **298**, 50 (1993).
[15] Y. Wang, M. J. Bronikowski, and R. J. Hamers, Surf. Sci. **311**, 64 (1994).
[16] C. Lutterloh, M. Wickleinb, A. Dingerb, J. Bienera, and J. Küppers, Surf. Sci. **498**, 123 (2002).
[17] S. Kulkarni, S. Gates, B. Scott, and H. Sawiri, Surf. Sci. **239**, 13 (1990).
[18] L. Q. Xia, M. E. Jones, N. Maity, and J. R. Engstrom, J. Chem. Phys. **103**, 1691 (1995).
[19] J. Shi, E. S. Tok, and H. C. Kang, J. Chem. Phys. **127**, 164713 (2007).
[20] R. W. Price, E. S. Tok, and J. Zhang, Phys. Rev. B **59**, R5292 (1999).
[21] J. Ku Kang and C. B. Musgrave, Phys. Rev. B **64**, 245330 (2001).
[22] F. C. H. Lim, E. S. Tok, and H. C. Kang, Phys. Rev. B **74**, 205333 (2006).
[23] J. P. Perdew, K. Burke, and M. Ernzerhof, Phys. Rev. Lett. **77**, 3865 (1996).
[24] R. D. Smardon and G. P. Srivastava, J. Chem. Phys. **123**, 174703 (2005).
[25] M. Iannuzzi, A. Laio, and M. Parrinello, Phys. Rev. Lett. **90**, 238302 (2003).
[26] A. Laio, A. Rodriguez-Fortea, F. L. Gervasio, M. Ceccarelli, and M. Parrinello, J. Phys. Chem. B **109**, 6714 (2005).
[27] G. Henkelman and H. Jónsson, J. Chem. Phys. **113**, 9978 (2000).
[28] P. Giannozzi *et al.*, http://www.quantum-expresso.org.
[29] CPMD, Copyright IBM Corp 1990–2008, Copyright MPI für Festkörperforschung Stuttgart 1997–2001, http://www.cpmd.org/.
[30] R. Car and M. Parrinello, Phys. Rev. Lett. **55**, 2471 (1985).
[31] N. Troullier and J. L. Martins, Phys. Rev. B **43**, 1993 (1991).
[32] D. Vanderbilt, Phys. Rev. B **41**, 7892 (1990).
[33] M. Ceriotti and M. Bernasconi, Phys. Rev. B **76**, 245309 (2007).
[34] S. Cereda, M. Ceriotti, F. Montalenti, M. Bernasconi, and L. Miglio, Phys. Rev. B **75**, 235311 (2007).
[35] Y. Okada and Y. Tokumaru, J. Appl. Phys. **56**, 314 (1984).
[36] A. Laio and M. Parrinello, Proc. Natl. Acad. Sci. U.S.A. **99**, 12562 (2002).
[37] A. Laio and F. L. Gervasio, Rep. Prog. Phys. **71**, 126601 (2008).
[38] W. G. Hoover, Phys. Rev. A **31**, 1695 (1985).
[39] G. J. Martyna, M. L. Klein, and M. Tuckerman, J. Chem. Phys. **97**, 2635 (1992).
[40] G. Henkelman, B. P. Uberuaga, and H. Jónsson, J. Chem. Phys. **113**, 9901 (2000).
[41] See EPAPS Document No. E-PRBMDO-79-026916 for a movie of metadynamics trajectory, and a discussion of Brillouin-zone

sampling issues. For more information on EPAPS, see http://www.aip.org/pubservs/epaps.html.

[42] G. Henkelman and H. Jónsson, J. Chem. Phys. **111**, 7010 (1999).

[43] G. S. Hwang, Surf. Sci. **465**, L789 (2000).

[44] A. Robinson Brown and D. J. Doren, J. Chem. Phys. **109**, 2442 (1998).

[45] S. P. Walch, S. Ramalingam, S. Sriraman, E. S. Aydil, and D. Maroudas, Chem. Phys. Lett. **344**, 249 (2001).

[46] D. R. Bowler and C. M. Goringe, Surf. Sci. **360**, L489 (1996).

[47] S. Hong and M. Y. Chou, Phys. Rev. B **58**, R13363 (1998).

[48] S. Cereda, F. Montalenti, M. Cogoni, D. Branduardi, M. W. Radny, P. V. Smith, and L. Miglio, Surf. Sci. **600**, 4445 (2006).

[49] T. Hashizume, H. Kajiyama, Y. Suwa, S. Heike, S. Matsuura, J. Nara, and T. Ohno, Appl. Surf. Sci. **216**, 15 (2003).

[50] S. Cereda, F. Zipoli, M. Bernasconi, L. Miglio, and F. Montalenti, Phys. Rev. Lett. **100**, 046105 (2008).

[51] P. Gupta, V. L. Colvin, and S. M. George, Phys. Rev. B **37**, 8234 (1988).

[52] J. H. G. Owen, K. Miki, D. R. Bowler, C. M. Goringe, I. Goldfarb, and G. A. D. Briggs, Surf. Sci. **394**, 79 (1997).

[53] A. P. Smith, J. K. Wiggs, H. Jónsson, H. Yan, L. R. Corrales, P. Nachtigall, and K. D. Jordan, J. Chem. Phys. **102**, 1044 (1995).

[54] J. Tersoff and D. R. Hamann, Phys. Rev. B **31**, 805 (1985).

[55] X. Tan and G. W. Yang, Appl. Phys. Lett. **93**, 061902 (2008).